Large Eddy Simulation of Fuel Sprays using the Eulerian Mesoscopic Approach. Validations in realistic engine conditions

L. Martinez[*,1], A. Vié[1], S. Jay[1], A. Benkenida[1] and B. Cuenot[2]
[1]IFP, 1&4 av. de Bois-Préau, 92852 Rueil-Malmaison Cedex - FRANCE
[2]CERFACS, 42 av. G. Coriolis, 31057 Toulouse Cedex 1 - FRANCE

Abstract

The main objective of this work is to assess the accuracy of the Large Eddy Simulation (LES) of fuel sprays in realistic engine conditions, using an Eulerian-Eulerian approach. For this purpose, numerical results of spray penetration are compared to experimental results in high pressure cells. The liquid and the gas phases are solved using conservation equations, and interact through source terms for mass, momentum and energy exchanges. The gas phase, composed of air and fuel vapour, is solved by compressible Navier-Stokes equations, whereas the liquid phase, *i.e.* the fuel injected, is solved using the Mesoscopic Eulerian Formalism (MEF) developed by Février et al. [J. Fluid Mechanics 2005]. Initially developed for dilute sprays, this formalism was then extended to dense sprays by Martinez et al. [ILASS 2007], taking into account collisions between droplets. These developments were introduced in AVBP, a parallel CFD code co-developed by IFP and CERFACS, and specially dedicated to LES. In order to simulate a Diesel spray, the methodology proposed by Martinez et al. [submitted to FUEL 2008] is used. An injector model is combined to conservation equations to obtain inflow turbulent boundary conditions, called DITurBc, at a given distance downstream from the nozzle exit. This strategy allows to perform LES calculations with reasonable CPU times because it avoids the simulation of complex phenomena, especially cavitation and primary break-up of the liquid core, that occur very close to the nozzle exit. Diesel spray simulations are performed and compared to experimental data in a high pressure vessel. The gas contained in the vessel is pressurised at 1,5 or 3 MPa with temperatures respectively of 800 and 400 K. Three injection pressures are tested : 40, 80 and 150 MPa. The LES calculations reproduce very accurately the evolution of the liquid fuel penetration for all cases. Comparisons between experimental shadowgraphs and 3D visualizations, show that the spray angle and volume are also well estimated by the LES. Evaporating sprays are then considered and results are again in good agreement with measurements for both liquid and vapour penetrations. Furthermore, it is verified that the numerical results are grid independent, which is a great benefit of the two-fluid model and confirms the quality of the LES.

Introduction

The Large Eddy Simulation (LES) technique is a promising tool for the prediction of cycle-to-cycle variability in Internal Combustion (IC) Engines. In particular, its capacity to resolve large scale vortices and to predict the interaction between droplets and air (the carrier phase) is of great interest for spray simulations [1], a key point for the prediction of the flow and the flame inside the chamber. This work is a contribution to the prediction of IC Engines by LES. It is devoted to Diesel like sprays and uses an Eulerian-Eulerian approach, preferred to a Lagrangian particle tracking method for its potential to model complex industrial two-phase flows with high particles load and high computational efficiency on massively parallel computers. Eulerian approaches for the dispersed phase however raise a number of modelling issues and this is studied in parallel work [2]. The present paper is devoted to the validation and analysis of the 3D LES simulation of realistic high pressure Diesel injections. The AVBP code [3] is used for the simulations. It solves the compressible Navier Stokes equations for reactive two-phase flows using low dissipation schemes adapted to LES. It allows to simulate monodisperse or polydisperse evaporating sprays.

[*]Corresponding author: lionel.martinez@ifp.fr

Equations and models for the two-fluid model

The simulations presented in this paper are performed without atomization nor coalescence. The phases are two-way coupled via drag force.

A. The Mesoscopic Eulerian Formalism

The Eulerian liquid conservation equations are based on the MEF developed by [4]. Inspired by the gas kinetic theory [5], it defines conservation equations, starting from the Boltzmann equation [6]. The key point of this formalism is the decomposition of particles velocities v_p into a correlated part V_p, common to all particles at a given location and a given time, and an uncorrelated part v'_p, proper to each particle. After statistical averaging of the particles motion over a large number of realizations (conditioned by one realization of the gas phase), and after the LES filtering procedure [7], [8] , the filtered equations for the liquid phase become [9]:

$$\frac{\partial}{\partial t}\rho_l \overline{\alpha_l} + \frac{\partial}{\partial x_i}\rho_l \overline{\alpha_l}\widehat{U}_{l,i} = \Gamma_l \tag{1}$$

$$\frac{\partial}{\partial t}\overline{n_l} + \frac{\partial}{\partial x_i}\overline{n_l}\widehat{U}_{l,i} = 0 \tag{2}$$

$$\frac{\partial}{\partial t}\rho_l \overline{\alpha_l} U_{l,i} + \frac{\partial}{\partial x_j}\rho_l \overline{\alpha_l}\widehat{U}_{l,i}\widehat{U}_{l,j} = \widehat{F}_{drag} + \frac{\partial}{\partial x_j}\widehat{\delta\Sigma}_{l,ij} - \frac{\partial}{\partial x_j}T_{l,ij} + \Gamma_l.\widehat{U}_{l,i} \tag{3}$$

$$\frac{\partial}{\partial t}\rho_l \overline{\alpha}_l \widehat{\delta\theta}_l + \frac{\partial}{\partial x_i}\rho_l \overline{\alpha}_l \widehat{\delta\theta}_l \widehat{U}_{l,i} = -\frac{2\rho_l \overline{\alpha}_l}{\tau_p}\widehat{\delta\theta}_l - \rho_l \overline{\alpha}_l \frac{1-e^2}{3\tau_c}\widehat{\delta\theta}_l + \left(\widehat{\delta\Sigma}_{l,ij} - T_{l,ij}\right)\frac{\partial}{\partial x_j}\widehat{U}_{l,i} - \frac{\partial}{\partial x_j}\rho_l \overline{\alpha}_l \widehat{\delta K}_{l,iij} + \widehat{\delta\theta}_l.\Gamma_l \tag{4}$$

where α_l is the liquid volume fraction, n_l the particle number density, $\widehat{U}_l$ the filtered correlated velocity of the MEF, $\widehat{\delta\theta}_l$ the Random Uncorrelated Energy (RUE) related to the uncorrelated velocity, $\widehat{F}_{drag}$ is the drag force and Γ is the mass source term due to evaporation modeled by the classical Spalding model [10]. The first two terms on the right hand side of Eq.(4) are the dissipation of RUE respectively by drag and by inelastic collisions. The third term is the production of RUE by shear and compression and by transfer from subgrid energy. The subgrid scale tensor $T_{l,ij}$ is modeled following [7], [8] using a Smagorinsky-Yoshizawa model. The filtered stress tensor $\widehat{\delta\Sigma}_{l,ij}$ may be decomposed into a kinetic contribution corresponding to the transport of uncorrelated motion, and a collisional contribution associated to the transfer of uncorrelated motion by collisions. The principles and development of the models have been presented and validated in the context of simple shear dense suspensions [11] and have been reviewed by [12]. The stress tensor $\widehat{\delta\Sigma}_{l,ij}$ is obtained via a Boussinesq hypothesis for the deviatoric part and the diffusive term $\widehat{\delta K}_{l,iij}$ is modeled by a diffusivity law. These tensors read :

$$\delta\hat{\Sigma}_{l,ij} = -\left(\frac{2}{3}\rho_l \overline{\alpha}_l \widehat{\delta\theta}_l - P_{coll} + \xi_{coll}\frac{\partial}{\partial x_k}\widehat{U}_{l,k}\right)\delta_{ij} + \left(\hat{\nu}_{kin,c} + \hat{\nu}_{coll}\right)\left(\frac{\partial\widehat{U}_{l,i}}{\partial x_j} + \frac{\partial\widehat{U}_{l,j}}{\partial x_i} - \frac{\partial\widehat{U}_{l,k}}{\partial x_k}\frac{\delta_{ij}}{3}\right) \tag{5}$$

$$\widehat{\delta K}_{l,iij} = -\left(\hat{\kappa}_{kin,c} + \hat{\kappa}_{coll}\right)\left(\frac{\partial\widehat{\delta\theta}_l}{\partial x_j}\right) \tag{6}$$

where the kinetic viscosity $\hat{\upsilon}_{kin,c}$ and diffusivity $\hat{\kappa}_{kin,c}$ are defined as:

$$\hat{\nu}_{kin,c} = \frac{\tau_p}{3}\widehat{\delta\theta}_l\left(1+\overline{\alpha}_1 g_0\frac{2}{5}(1+e)(3e-1)\right)\Bigg/\left(1+\frac{\tau_p}{\tau_c}\frac{(1+e)(3-e)}{10}\right) \tag{7}$$

$$\hat{\kappa}_{kin,c} = \frac{2}{3}\widehat{\delta\theta}_l\left(1+\overline{\alpha}_1 g_0\frac{3}{5}(1+e)^2(2e-1)\right)\Bigg/\left(\frac{9}{5\tau_p}+\frac{(19-33e)(1+e)}{100\tau_c}\right) \tag{8}$$

The drag force $\widehat{F}_{drag}$, the relaxation and the collision time scales, respectively τ_p and τ_c , are defined as:

$$\widehat{F}_{drag,i} = \frac{\rho_l \overline{\alpha}_l}{\tau_p}\left(\widehat{U}_{g,i} - \widehat{U}_{l,i}\right) \quad \text{where} \quad \tau_p = \frac{\rho_l d^2}{18\mu_g}, \quad \text{and} \quad \tau_c = \frac{d}{24 g_0 \overline{\alpha}_l}\sqrt{\frac{3\pi}{\widehat{\delta\theta}_l}} \tag{9}$$

$$\text{with} \quad g_0 = \left(1 - \frac{\overline{\alpha}_l}{\alpha_m}\right)^{-2.5\alpha_m} \text{ following [12]} \quad \text{and } \alpha_m = 0.64 \tag{10}$$

where e is the elasticity coefficient, set arbitrarily here to 0.8. The collisional viscosity $\hat{\upsilon}_{coll}$, the collisional diffusivity $\hat{\kappa}_{coll}$, the collisional pressure P_{coll} and the bulk viscosity ξ_{coll} are set as:

$$\hat{\nu}_{coll} = \frac{4}{5}\overline{\alpha}_l \, g_0 (1+e)\left(\hat{\nu}_{kin,c} + d\sqrt{\frac{2\widehat{\delta\theta}_l}{3\pi}}\right), \quad \hat{\kappa}_{coll} = \overline{\alpha}_l \, g_0 (1+e)\left(\frac{6}{5}\hat{\kappa}_{kin,c} + \frac{4}{3}d\sqrt{\frac{2\widehat{\delta\theta}_l}{3\pi}}\right) \tag{11}$$

$$P_{coll} = \frac{4}{3}\rho_l \overline{\alpha}_l^2 g_0 (1+e)\widehat{\delta\theta}_l, \quad \xi_{coll} = \frac{4}{3}\rho_l \overline{\alpha}_l^2 g_0 (1+e) d\sqrt{\frac{2\widehat{\delta\theta}_l}{3\pi}} \tag{12}$$

The previous equations may be seen as an extension of the work of [4] to include collisions. When the liquid volume fraction tends to 0 the closure models of [4] are retrieved.

B. Gas phase equations

Equations for the gas phase are the classical filtered Navier-Stokes equations with two-way coupling terms :

$$\frac{\partial}{\partial t}\rho_g + \frac{\partial}{\partial x_i}\rho_g \widehat{U}_{g,i} = \Gamma_g = -\Gamma_l \tag{13}$$

$$\frac{\partial}{\partial t}\rho_g \widehat{U}_{g,i} + \frac{\partial}{\partial x_j}\rho_g \widehat{U}_{g,i}\widehat{U}_{g,j} = \widehat{F}_{drag} - \frac{\partial}{\partial x_i}\overline{P} + \frac{\partial}{\partial x_j}\rho_g \nu_g \widehat{\sigma}_{g,ij} + \frac{\partial}{\partial x_j}T_{g,ij} + \Gamma_g . \widehat{U}_{l,i} \tag{14}$$

$$\frac{\partial}{\partial t}\rho_g \widehat{E}_g + \frac{\partial}{\partial x_i}\widehat{U}_{g,i}\left(\rho_g \widehat{E}_g + \overline{P}\right) = \widehat{F}_{drag}.\widehat{U}_{l,i} + \frac{\partial}{\partial x_j}\left(\rho_g \nu_g \widehat{\sigma}_{g,ij}\right)U_{g,i} + \frac{\partial}{\partial x_j}\overline{Q}_{g,j} + \left(\widehat{U}_{g,i}\widehat{U}_{l,i}\right).\Gamma_g \tag{15}$$

where $\widehat{\sigma}_{g,ij}$ is the filtered strain tensor of the gas phase, $T_{g,ij}$ is the subgrid scale tensor modeled by a viscous assumption via the dynamic Smagorinsky model [14]. The only coupling between the two phases is the drag force in a two-way coupling and it is assumed that the subgrid model is not modified by the droplets. This set of equations does not take into account the volume effect induced by the presence of the liquid phase. This avoids the coupling between liquid and gas thermo-acoustic instabilities that would need to reconsider boundary conditions treatment. However the regions of dense spray where a volume correction is needed are very limited and the above simplification is expected to have only weak effects.

Results and Discussion

A. High pressure vessel

Realistic Diesel engine conditions were reproduced by IFP [15], [16] in a high pressure vessel. Using n-dodecane, liquid and vapour penetrations were measured and shadowgraphs were obtained for four test cases: three non-vaporizing sprays, with injection pressures varying from 40 MPa to 150 MPa, and one vaporizing spray. The conditions of all test cases, named T4P4, T4P8, T4P15 and T8P4 in reference to their temperature and injection pressure, are summarized in Table 1. The injection system is the same for all cases and the nozzle diameter is 200 µm..

B. Mesh and boundary conditions

A tetrahedral 3D mesh is used (Table 2). All simulations are computed with the AVBP LES code using the third order low dissipation scheme TTGC [17]. The methodology proposed by Martinez et al. [18] for Diesel injection is used to handle the liquid inlet boundary condition. It combines an injector model and conservation equations to obtain inflow turbulent boundary conditions, called DITurBc, at a given distance downstream from the nozzle exit. This strategy allows to perform LES calculations with reasonable CPU times as it avoids the simulation of complex

phenomena, especially cavitation and primary break-up of the liquid core, that occur very close to the nozzle exit [18]. The shifted boundary conditions are imposed on the base surface of a cone, added to the mesh, and representing the non-simulated region (Figure 5). The profiles of droplet velocities, diameter and liquid volume fraction at the boundary conditions are supposed to be Gaussian. Profiles of velocities and volume fraction are fully determined by the model but the maximum droplet diameter is a user-defined parameter. One difficulty is then to find the correct maximum droplet diameter. Here it is set to 20 μm. In order to evaluate the impact of this free parameter, a sensitivity study is proposed for the cases T4P4 and T8P4.
In addition, in order to evaluate grid dependency and convergence, two other meshes have been tested, with characteristics edge lengths 0.7Δ and 1.2Δ, where Δ is the characteristic edge length of the first reference mesh.

C. Results of spray simulations

The results of the LES Euler-Euler simulations are compared to the experimental data in terms of penetration and spray angle. Figure 1 presents the results for the non-evaporating sprays T4P4, T4P8 and T4P15. Good agreement with the experiment is obtained for all conditions. The decrease of the slope of the penetration is particularly well reproduced, although no atomization processes were included. Results are less satisfactory for the case T4P4 but this low pressure case is the less relevant to industrial applications. To see the influence of the inlet droplet diameter, Figure 2 and 3 present the penetrations obtained with a maximum droplet diameter of 10 μm compared to 20 μm for the T4P4 and T8P4 cases respectively. In both cases the smaller diameter leads to a smaller penetration, below the experimental measurements, but the difference is low and in the case T4P4 is of the same order than the experimental error (3mm). For the vaporizing spray T8P4 the same conclusions hold for the vapour penetration: with d=10 μm, the vapour result is very close to the case d=20 μm showing again that the diameter has a low effect on penetration. The liquid penetration is more under-estimated than in the previous case, by 5 to 8 mm. However in engine calculations, the most important quantities to estimate are the vapour penetration and air entrainment. The liquid penetration is less important so that the uncertainty on inlet diameter may not be so problematic. In both cases, the value 20 μm seems to be the best choice.
The sensitivity to the grid resolution for T4P4 is investigated in Figure 4. The spray penetration seems to be very little sensitive to the grid resolution. This is clearly an advantage of the two-fluid MEF approach compared to the Lagrangian one. In addition, this shows the quality and accuracy of the LES, as the decrease of penetration is due to the expansion of the spray interacting with turbulence. The LES simulations are grid converged, with a subgrid energy in the dissipation range and low compared to the resolved energy.
The spray itself is viewed through iso-surfaces of droplet diameter (d=3μm). Indeed in a non evaporating case, the spray may be identified by the droplets diameter: high values corresponds to the spray, low values correspond to no spray (in Eulerian formulations liquid fields are defined everywhere). Diameter iso-surfaces are shown in Figure 6 for T4P8 and compared to experimental shadowgraphs at different times. The overall spray volume is qualitatively in agreement with the experiment. The spray opening is also well reproduced by the simulation. Close to the nozzle exit, the spray angle keeps a relatively low value and the spray stays narrow, until a transition to a larger angle and a fast opening of the spray. The numerical iso-surfaces show well that this sudden spray angle increase is due to large scale vortices that grow with the distance to the nozzle exit. This change of spray angle may correspond to the transition to a turbulent free jet behavior. The location of transition is found closer to the nozzle exit in the simulation, where the spray seems to be destabilized sooner. This may be due to different phenomena and should be analyzed in detail.

Conclusions

Accurate numerical results for spray penetrations in both evaporating and non-evaporating cases were obtained with the Mesoscopic Eulerian Formalism LES, for different injection pressures, and in realistic engine conditions. The good agreement between experiments and simulations in terms of spray penetration, volume and angle, validate the methodology and the models. A sensitivity study on the injected droplet diameter, a free parameter of the model, shows that it has only a weak effect on spray penetration in the considered test cases, mainly on the liquid penetration in the vaporizing spray. Grid convergence was reached, and LES results were almost no sensitive to grid resolution, which is a great advantage of two-fluid methods. Another original result is that LES is able to reproduce experiments with adequate accuracy, without taking into account atomization nor coalescence. This indicates that these two phenomena, that play a major role in the very first instants of spray formation (modeled in the present LES), are not so important in the later times. Additional investigation on the role of polydispersion and atomization is currently ongoing.

Nomenclature

d droplet diameter
e inelasticity coefficient
E total energy
n_l droplet number density
U velocity
α_l liquid volume fraction
ρ density
$\delta\theta_l$ random uncorrelated energy
Γ mass source term due to evaporation
κ diffusivity
ν viscosity
τ_c collision time scale
τ_p relaxation time scale
Δ characteristic edge length

Subscripts
g gas
l liquid
$_{kin,c}$ kinetic
$_{coll}$ collisional

Superscripts
^ Favre filtered variable
- filtered variable

References

1. Bellan, J., *Atomization and Sprays* 10:409-425 (2000)
2. Vié, A., Martinez, L., Jay, S., Benkenida, A. and Cuenot, B., *11th ICLASS,* Vail, Colorado, USA, July 2009
3. Moureau, V., Lartigue, G., Sommerer, Y.,Angelberger, C., Colin, O., and Poinsot, T., *J. Comp. Physics* 202: 710-736 (2005).
4. Février, P., Simonin, O., and Squires, K., *Journal of Fluid Mechanics* 533 (2005).
5. Chapman, S., and Cowling, T., *The mathematical theory of non-uniform gazes*, Cambridge Univ. Press, 1939.
6. Kaufmann, A., Moreau, M., Simonin, O., and Helie, J., *J. Comp. Physics* 227: 6448-6472 (2008).
7. Moreau, M., Bédat, B., and Simonin O., *18th ILASS Americas,* Irvine, US, 2005
8. Riber, E., M. Moreau, O. Simonin, and B. Cuenot*, FEDSM2006,* Miami, Florida, US, 2006.
9. Martinez, L., Benkenida, A., and Cuenot, B., *21th ILASS – Europe Meeting*, Muğla, Turkey, 2007.
10. Spalding, D.B.*, Fourth Symp. (Int.) on Combustion,* The Combustion Institute, Pittsburgh, 1953.
11. Boelle, A., Blazer, G., and Simonin, O., *Sixth ASME Gas-Solid Flows Symposium*, Hilton Head Island, US, 1995.
12. Peirano, E., and Leckner, B., *Progress in Energy and Combustion Science* 24: 259-296 (1996).
13. Lun, C., and Savage, B., *Acta Mechanica.* 63: 15-44, (1986)
14. Germano, M., Piomelli, U.; Moin, P. and Cabot, W., *Physics of Fluids* 3: 1760-1765 (1991).
15. Vanhemelryck, J., *IFP Technical report* 1996
16. Verhoven, D., Vanhemelryck, J. and Baritaud, T., *SAE technical paper 981069* (1998)
17. Colin, O. and Rudgyard, M., *J. Comp. Physics* 162(2): 338-371 (2000)
18. Martinez, L., Benkenida, A., and Cuenot, B., *submitted to FUEL* (2008).

Table 1. Conditions of the four injection cases

Name	Injection Pressure (MPa)	Temperature (K)	Density (kg/m^3)	Bernoulli velocity (m/s)
T4P4	40.0	387.0	387.0	340
T4P8	40.0	387.0	387.0	480
T4P15	150.0	387.0	387.0	650
T8P4	40.0	800.0	800.0	340

Table 2. Numerical Parameters.

Node number	Element type	Minimum edge length (μm)	Physical time (s)	CPU Time (64 proc.)	Numerical scheme
340 000	Tetrahedral	80	2. 10^{-3}	20 h	TTGC [17]

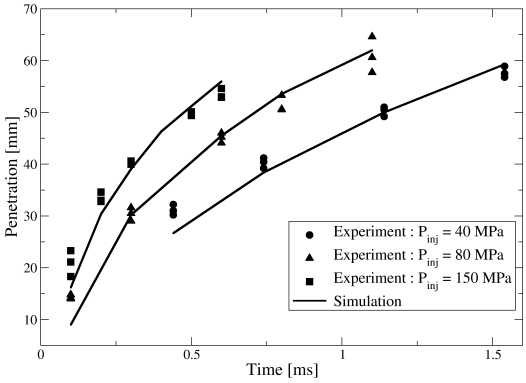

Figure 1. Comparison of penetration between simulation and experiment for cases T4P4, T4P8 and T4P15.

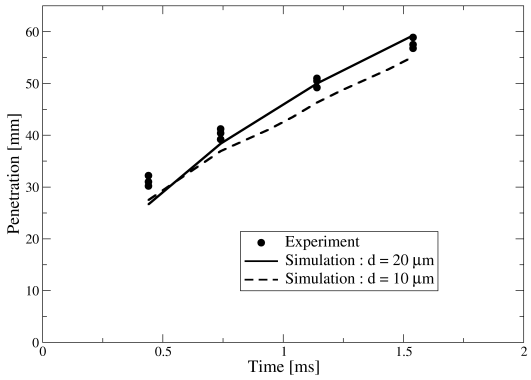

Figure 2. Comparison of penetration between simulation and experiment for T4P4 case: Effect of maximum droplet diameter.

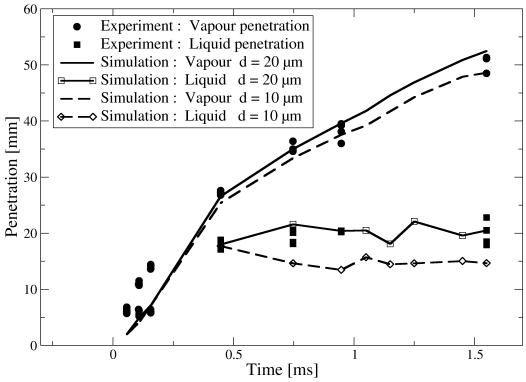

Figure 3. Comparison of vapour and liquid penetrations between simulation and experiment for T8P4 case.

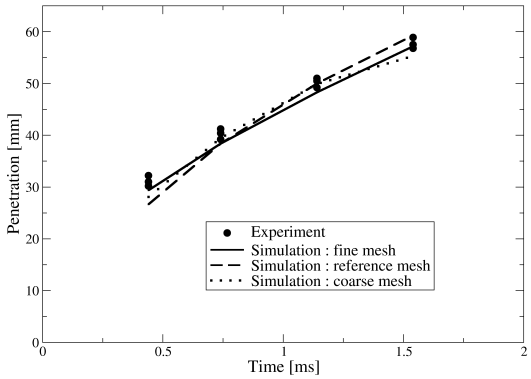

Figure 4. Comparison of penetration between simulation and experiment for T4P4 case: Effect of grid resolution.

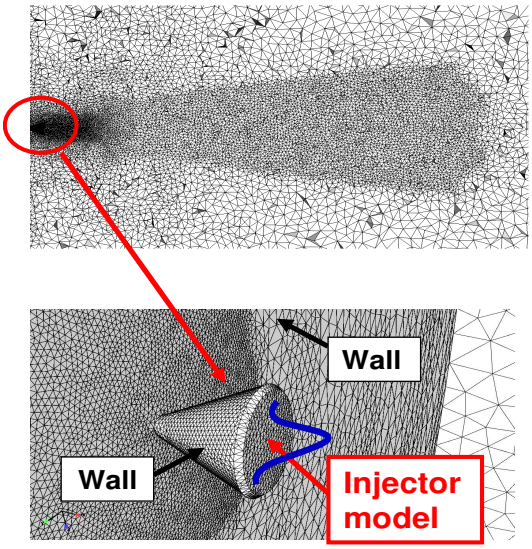

Figure 5. Cross section of the mesh and view of the cone dedicated to the shifted boundary condition

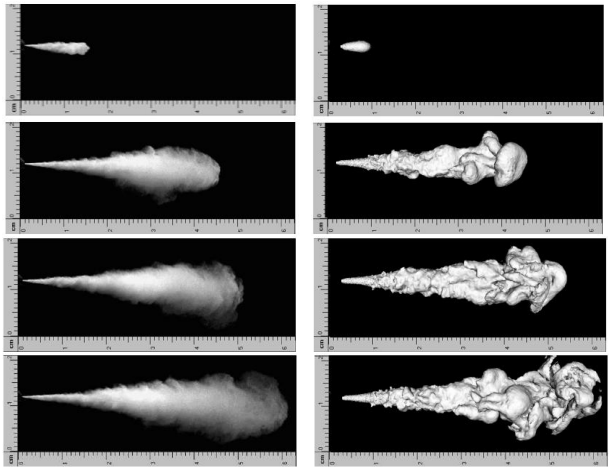

Figure 6. Visualization of the spray for the T4P8 case. Comparison between experiment (left) and iso-surfaces of droplet diameter (d=3µm) obtained with LES (right) at different times (t=0.1ms, 0.6ms, 0.8ms and 1.1ms)